Applied Physics B (2020) 126:135
https://doi.org/10.1007/s00340-020-07490-9

**Applied Physics B**
**Lasers and Optics**

# Preparation of Ag@ZnO core–shell nanostructures by liquid-phase laser ablation and investigation of their femtosecond nonlinear optical properties

**Shuai Zhang[1] · Heng Lu[1] · Guanghao Rui[1] · Changgui Lv[1] · Jun He[2] · Yiping Cui[1] · Bing Gu[1,3]**

Received: 12 December 2019 / Accepted: 11 July 2020 / Published online: 19 July 2020


**Abstract**
Ag@ZnO core–shell nanostructures, ZnO nanoparticles (NPs), and Ag NPs were synthesized by laser ablation in water using 8 ns, 1064 nm, and 50 mJ/pulse. The structural, morphological, componential, and optical properties of as-synthesized NPs were examined by X-ray diffraction, transmission electron microscopy, electron diffraction spectrum, and ultraviolet–visible absorption, respectively. The third-order nonlinear optical properties of aqueous dispersions of three NPs were characterized by performing Z-scan experiments with femtosecond laser pulses at 800 nm. It is shown that three NPs exhibit the positive refractive nonlinearity in the absence of nonlinear absorption and the third-order nonlinear refraction index increases in the order of NPs ZnO < Ag < Ag@ZnO. The results indicate that the Ag@ZnO core–shell nanostructure is a promising candidate for applications in ultrafast all-optical switching.

## 1 Introduction

In the past decade, multicomponent core–shell composite nanostructures [1, 2] have received extensive attention because of their widespread applications in surface-enhanced Raman scattering [3], catalysis and electrocatalysis [4], electrochemical sensor [5], photonic crystals [6], etc. Up to now, many methods have been reported to synthesize core–shell nanostructures, such as microwave-assisted hydrothermal method [7], polyol reduction [8], and vacuum evaporation deposition [9]. These methods have the advantages of high efficiency. However, the synthesis process is relatively complex and it is difficult to avoid the introduction of impurities. Compared with the above-mentioned methods, pulsed laser ablation in liquid solutions (PLAL) has the advantages of simple, short preparation period, and a wide range of applications [10, 11]. Importantly, the synthesized nanomaterials by this method are chemically pure. Moreover, the morphology and size of the synthesized nanoparticles can be manipulated by controlling the laser characteristic parameters (e.g., wavelength, pulse duration, repetition rate, and power) and the liquid-phase environments. A variety of nanomaterials have been synthesized by PLAL, including Ag and Au NPs [12, 13], alloy NPs [14], metal core–shell nanostructures [2], and metal/metal oxide semiconductor core/shell nanostructures [15].

As a class of multicomponent core–shell composite nanostructure, the noble metal/semiconductor core–shell composite NP (e.g., Ag@$SiO_2$ NPs [16], Ag@$TiO_2$ NPs [17], Ag@ZnO NPs [18]) has unique photophysical properties owing to the strong coupling exciton effect between the surface plasmon resonance (SPR) of the noble metal and the excitons of the semiconductors [19]. Interestingly, because of the intrinsic large optical nonlinearity of a composite material and the enhancement of local field of metal NPs, these metal NPs coated with transparent semiconductors exhibit strong third-order nonlinear optical effects [20], which have broad nonlinear photonic applications in nonlinear optical imaging [21], optical limiting [17], all-optical switching [22], and so on. In general, third-order optical nonlinearities of core–shell structured metal/semiconductor materials are influenced by the particle sizes and shapes, the dielectric constant, thermal conductivity, heat capacity

✉ Bing Gu
gubing@seu.edu.cn

[1] Advanced Photonics Center, Southeast University, Nanjing 210096, China

[2] School of Physics and Electronics, Central South University, Changsha 410012, China

[3] Collaborative Innovation Center of Light Manipulations and Applications, Shandong Normal University, Jinan 250358, China

of the composite system, as well as the synthesized method [23–25]. As such, many investigations focus on the optical nonlinearity of core–shell nanostructures [17, 26], since the complete understanding of these nonlinear effects is still incomplete. It is noteworthy that most of these investigations have been performed with nanosecond and picoseconds laser pulses [27]. However, there are few reports on the nonlinear optical properties of core–shell nanoparticles in the femtosecond regime.

In this work, we report a two-step PLAL method for the synthesis of Ag@ZnO core/shell nanostructures and investigate their femtosecond nonlinear optical properties. The structural, morphological, componential, and optical properties of as-synthesized NPs were characterized by X-ray diffraction (XRD), transmission electron microscopy (TEM), electron diffraction spectrum (EDS), and ultraviolet–visible (UV–Vis) absorption, respectively. The nonlinear optical properties of aqueous dispersions of NPs were studied by carrying out femtosecond-pulsed Z-scan measurements. It is found that NPs exhibit positive refractive nonlinearity in the absence of nonlinear absorption and the third-order nonlinear refraction index increases in the order of NPs ZnO < Ag < Ag@ZnO.

## 2 Experimental details

### 2.1 Preparation of NPs

To compare the photophysical properties of Ag@ZnO core–shell NPs with those of Ag and ZnO NPs under the same experimental conditions, we adopt the PLAL to synthesize ZnO NPs, Ag NPs, and Ag@ZnO core/shell NPs in deionized water. The core–shell nanostructures and single particles are synthesized by the two-step and one-step methods, respectively. It is noted that the distinct difference between the synthesis of particles (i.e., Ag and ZnO NPs) and core–shell NPs lies in the process and time of synthesis.

The experimental arrangement is illustrated in Fig. 1a. The metal plate (> 99.99%) was placed on the bottom of a glass vessel with 20-ml deionized water and then ablated by an Nd:YAG laser operating at a wavelength of 1064 nm with a pulse duration of 8 ns, a repetition rate of 10 Hz, and an energy of 50 mJ/pulse. The laser beam was focused on the metal plate by a convergent lens with a focal length of 100 mm.

The Ag@ZnO core–shell structures were synthesized by following a two-step method, as shown in Fig. 1b. First, a 2-mm-thick silver plate was placed on the bottom of a glass vessel which was located at 10 mm from the solution surface in the solution. The silver plate was continuously ablated for 60 min. Second, a zinc plate of the same size was ablated by the same laser with the same laser pulse energy in the

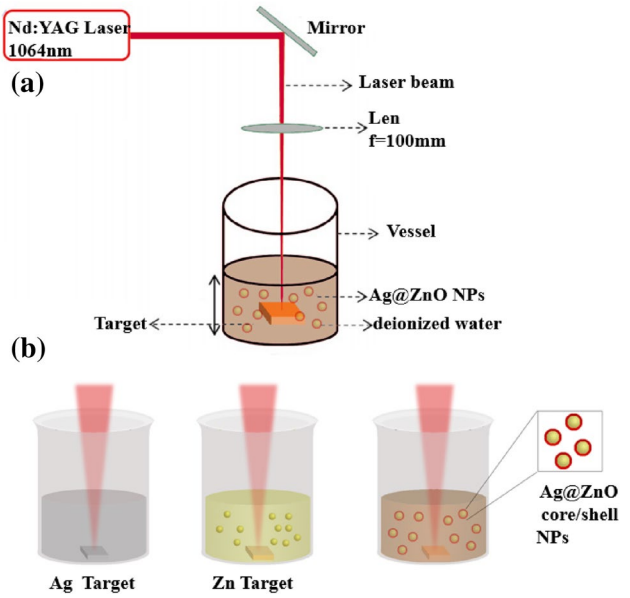


**Fig. 1** **a** Schematic diagram of the PLAL setup. **b** Synthesis process of the Ag@ZnO core–shell nanostructures

Ag colloid synthesized by the first step for 60 min with the aim of synthesizing the Ag@ZnO core–shell NPs. Ag NPs (or ZnO NPs) used for comparison were synthesized by the same laser at the same energy by ablation of a sliver (or zinc) plate in deionized water for 60 min. In addition, we determined the mass concentrations for aqueous suspensions of Ag, ZnO, and Ag@ZnO NPs to be $d_0 = 27.6$, 28.1, and 28.4 mg/ml, respectively.

### 2.2 Sample characterizations

The as-synthesized three NPs were confirmed and investigated by various characterization techniques as follows. The crystal phase analysis was performed on a German Bruker X-ray powder diffractometer using $CuK_\alpha$ radiation ($\lambda = 0.154056$ nm) at 40 kV and 30 mA in a $2\theta - \theta$ scanning mode. XRD patterns were recorded over a $2\theta$ range of 30°–80° at a step of 0.02°. The morphology and size distribution of the samples were inspected by TEM using a JEM-2100F electron microscope operated at the accelerating voltage of 120 kV. A standard procedure was followed to prepare the sample for the TEM analysis by dispersing the NPs in deionized water, and a drop of the aqueous suspension was put on the carbon-coated copper grid. The particle sizes were estimated from TEM images. The composition of NPs was characterized by the TEM–EDS using a JEM-2100F electron microscope. The UV–Vis linear absorption spectra of nanomaterial dispersions contained in 1-mm-thick quartz cells were detected at room temperature with a Shimadzu UV-3600 spectrophotometer.

### 2.3 Nonlinear optical characterization technique

The third-order nonlinear optical properties of the nanomaterial dispersions were investigated by a single-beam Z-scan technique [28]. The laser source for the Z-scan experiment was a Ti:sapphire regenerative amplifier (Coherent Inc.), operating at a wavelength of $\lambda = 800$ nm with a pulse duration of 170 fs and a repetition rate of 1 kHz. The laser pulses had near-Gaussian spatial and temporal profiles. The laser beam was focused by an achromatic lens with a focal length of 150 mm, producing the beam waist at the focus of $\omega_0 \simeq 15$ µm. To carry out the Z-scan measurements, the sample was scanned across the focus along the optical axis using a computer-controlled translation stage, while the transmitted pulse energies in the presence or absence of the far-field aperture were monitored by a detector, determining the closed- and open-aperture Z-scan traces, respectively. For the closed-aperture Z-scan measurements, the linear transmittance of the far-field aperture was kept at $S = 0.20$. In addition, the Z-scan measurement system was calibrated with carbon disulfide. The results indicate that the experimental uncertainty should be within ± 10%.

## 3 Results and discussion

### 3.1 Crystal structure

The phase and crystallographic structure can be identified by the XRD patterns of three NPs shown in Fig. 2. The black curve in Fig. 2 shows the XRD pattern of Ag NPs. It is shown that the powder XRD peaks at the $2\theta$ values of 38.3°, 45.50°, 64.1°, and 78.1° correspond to the crystalline planes of (111), (200), (220), and (311) of Ag NPs, respectively. These peaks are in agreement with the data of the card 04-0783 in the joint committee on powder diffraction standards (JCPDS) file of the face centred cubic structure of Ag.

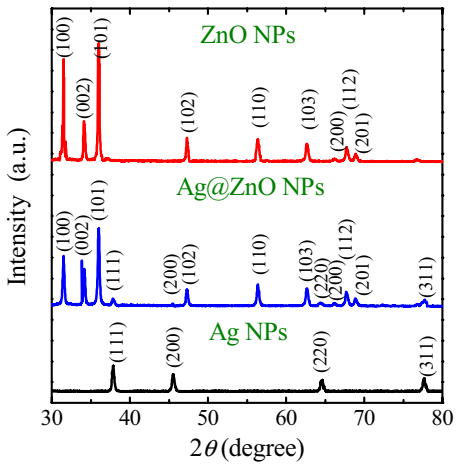


**Fig. 2** XRD patterns of as-prepared Ag, ZnO, and Ag@ZnO NPs

From the red curve shown in Fig. 2, one gets six peaks located at 31.5°, 34.18°, 36.02°, 47.34°, 56.34°, and 67.7°, which are attributed to the crystalline planes of (100), (002), (101), (102), (110), and (112) of ZnO NPs, respectively. All these XRD peaks of ZnO NPs are indexed to the hexagonal wurzite structure of ZnO (JCPDS card no. 36-1451). The results show that the ZnO NPs have good crystal quality.

The blue curve in Fig. 2 represents the XRD pattern of Ag@ZnO core–shell nanostructure. It is found that two sets of diffraction peaks, including XRD peaks of both Ag and ZnO, correspond to the face-centred structure of Ag (JCPDS card no. 04-0783) and hexagonal wurzite structure of ZnO (JCPDS card no. 36-1451). It is noteworthy that the diffraction peaks of the Ag core are weaker than those of pure Ag NPs, because the Ag core is completely covered by the ZnO shell. Compared to the diffraction peaks in Ag NPs and ZnO NPs, no noticeable shift in the diffraction peaks of Ag and ZnO in Ag@ZnO NPs is observed, indicating a strong interfacial interaction between Ag and ZnO to form a core–shell structure. In addition, absence of other impurity diffraction peaks suggests high purity of the Ag@ZnO core–shell nanostructure synthesized by liquid-phase laser ablation.

### 3.2 Morphology and size

The morphology and size distribution of the as-synthesized NPs are inspected by the TEM analysis. The corresponding results are presented in Fig. 3. It is found that the TEM images of the Ag and ZnO NPs shown in Fig. 3a1, a2 are almost spherical in two samples, no considerable aggregation took place for nanoparticles. The average diameters of Ag and ZnO NPs are estimated to be 20 and 65 nm, respectively. More importantly, the TEM image of Ag@ZnO NPs displayed in Fig. 3a3 reveals overall uniform spherical morphology. Moreover, the average diameter of Ag@ZnO NPs is measured to be 24 nm. Note that Fig. 3a3 shows the particle aggregation because the NPs are not dispersed uniformly enough [29]. In the linear and nonlinear optical measurements, ultrasonic NPs are used to ensure that the particles in deionized water are dispersed almost uniformly.

To gain an insight into the structure of a single particle, we measured the HRTEM images of three NPs shown in the second row of Fig. 3. The HRTEM images of Ag and ZnO NPs shown in Fig. 3b1, b2 indicate that they have a clear crystalline structure and a prevalently spherical shape. Interestingly, the HRTEM image of an Ag@ZnO particle displayed in Fig. 3b3 has the following characteristics: (1) there is an obvious shell with a thickness of ~ 4 nm coated on a core of ~ 20 nm in diameter; (2) the black core and the gray color are attributed to the Ag core and the ZnO shell, respectively. This color gradient arises from the difference of

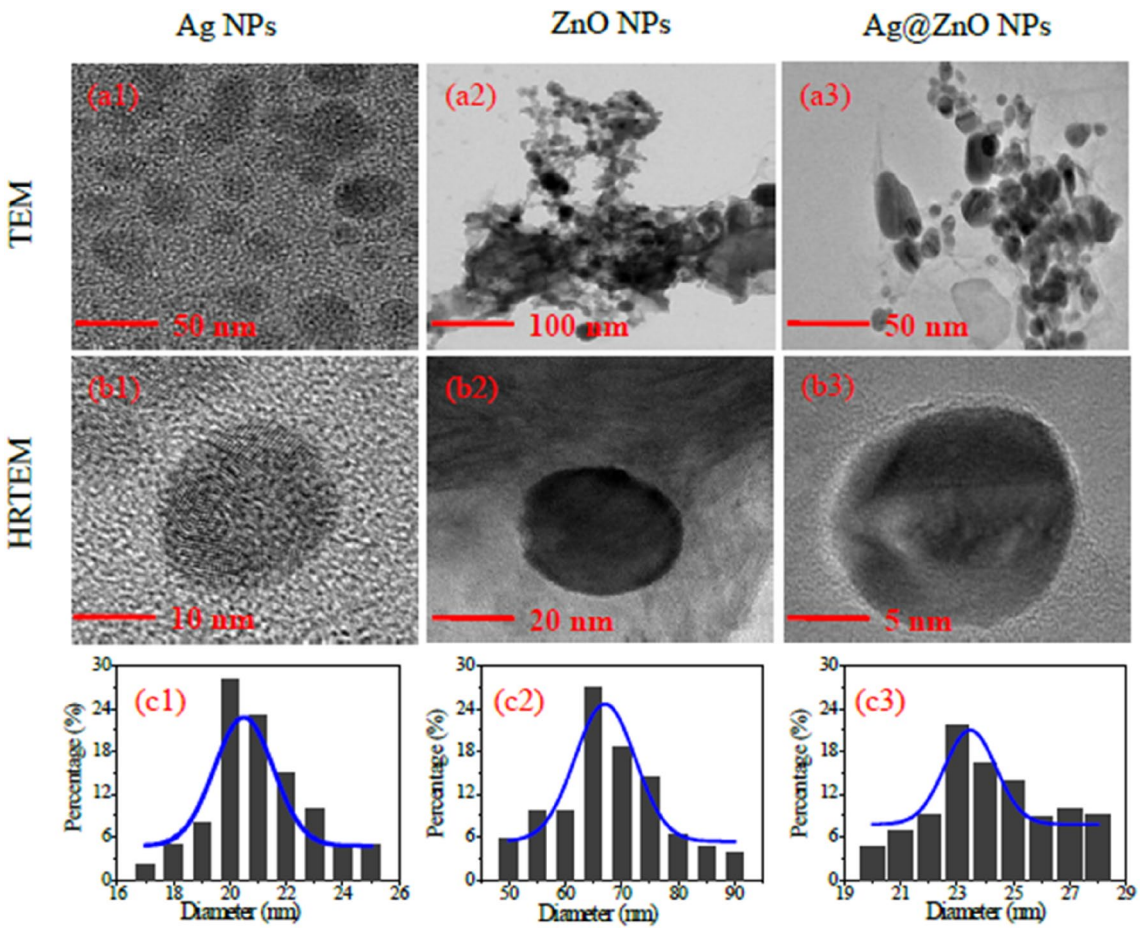


**Fig. 3** **a1**–**a3** TEM images, **b1**–**b3** HRTEM images, and **c1**–**c3** size distributions of Ag, ZnO, and Ag@ZnO NPs

the electron density between Ag (atomic number = 47) and Zn (atomic number = 30) [30]. Accordingly, the Ag core and ZnO shell are confirmed by HRTEM. This result suggests that the products of the two-step laser ablation method are indeed Ag@ZnO core–shell nanostructures.

The size distributions of Ag, ZnO, and Ag@ZnO NPs are counted as illustrated in the third row of Fig. 3. It is shown that the size distribution of the particle is nearly of Gaussian type. The diameters of the Ag, ZnO, and Ag@ZnO NPs are approximately 18–24, 50–85, and 20–28 nm, respectively.

### 3.3 Composition of nanoparticles

The EDS is used to further characterize the composition of as-synthesized NPs. Figure 4a–c show the EDS images of Ag, ZnO, and Ag@ZnO NPs, respectively. It is noted that the Cu and C elements are introduced because carbon film-coated copper mesh is used in the measurements. As shown in Fig. 4a, no other element peaks appear in the Ag NP, indicating that the sample is pure Ag nanostructure and is not doped with other substances. Analogously, the EDS spectra displayed in Fig. 4b, c reveal that both ZnO NP and Ag@ZnO core–shell nanostructure are pure, respectively.

### 3.4 Absorption spectra

The UV–Vis linear absorption spectra of Ag, ZnO, and Ag@ZnO NPs in deionized water are presented in Fig. 5a. Clearly, the linear absorption spectrum of Ag@ZnO core/shell nanostructure is not a simple superposition of those of Ag and ZnO NPs. The Ag NP has an intense SPR peak in the visible region, which is highly sensitive to its diameter and the optical and electronic properties of the surrounding environment [31]. As shown by the dotted line in Fig. 5a, Ag NPs exhibit an SPR peak at 402 nm owing to their small size [32]. Compared with that of Ag NPs, however, the SPR band of Ag@ZnO NPs is distinctly broadened and has a redshift by 24 nm, mainly because of the strong electronic coupling between the Ag core and ZnO shell [33, 34]. The electron transfer from Ag to ZnO in the Ag@ZnO core–shell nanostructure is due to the higher Fermi energy level of Ag than that of ZnO. This transfer results in deficiency of electrons

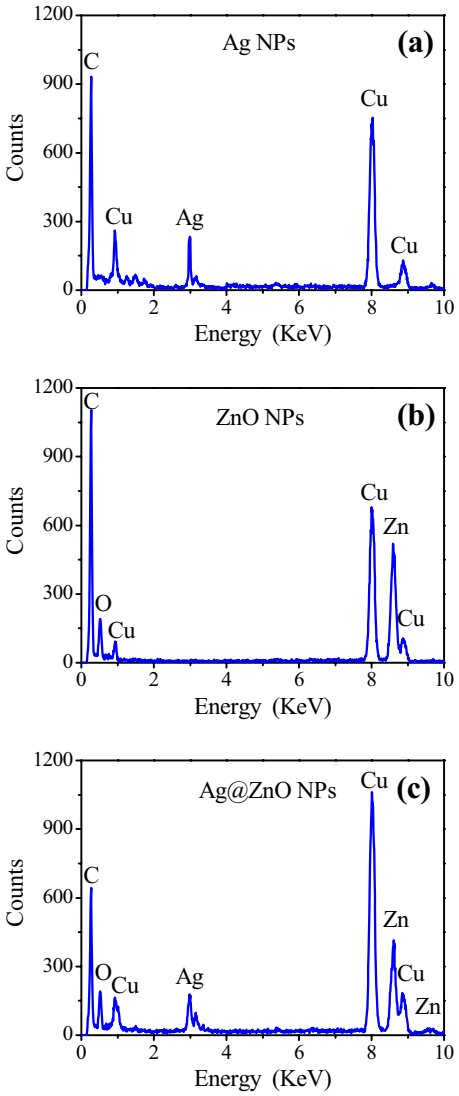


**Fig. 4** EDS images of **a** Ag NPs, **b** ZnO NPs, and **c** Ag@ZnO NPs

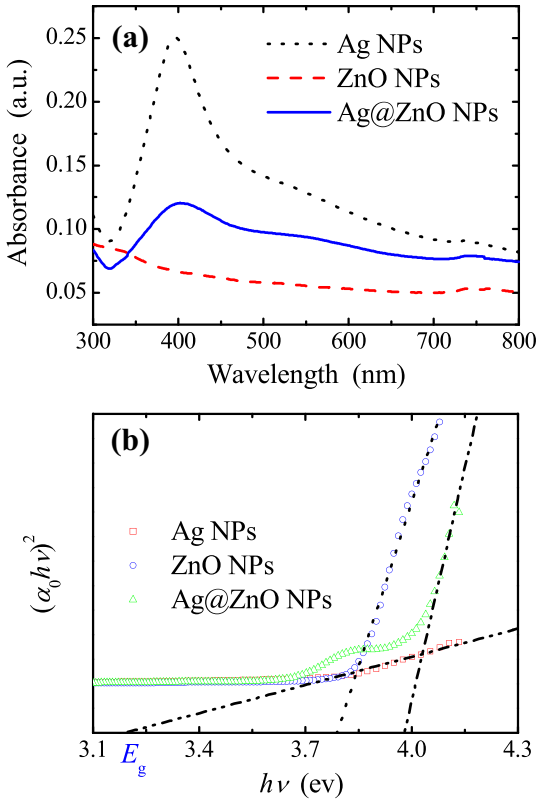


**Fig. 5** **a** Linear absorption spectra and **b** $(\alpha_0 h\nu)^2$ as a function of photon energy $h\nu$ for Ag, ZnO, and Ag@ZnO NPs

on the surface of Ag NP, leading to the redshift in the surface plasmon absorption [33, 35].

The optical bandgap $E_g$ of NPs can be estimated by extrapolation of the absorption edge with Tauc's formula $(\alpha_0 h\nu)^{2/n} = \text{Const}(h\nu - E_g)$, where $h\nu$ is the photon energy of excitation light and $n$ is determined by the characteristics of electron transitions between the valence and conduction bands in a material [36]. From the data shown in Fig. 5b, we obtain $n = 1$ and extrapolate $E_g = 3.23$, 3.78, and 3.94 eV for Ag, ZnO, and Ag@ZnO NPs, respectively. The results indicate that Ag, ZnO, and Ag@ZnO NPs, respectively, have a direct bandgap at the wavelength of 384, 328, and 314 nm. Alternatively, the $E_g$ value of NPs can be estimated by the empirical formula $E_g = 3.22 - 0.896/d + 2.86/d^2$, where $d$ is the diameter of the spherical NP in nanometers [37]. For example, we obtain $E_g = 3.18$ eV for Ag NPs with $d = 20$ nm, which is in agreement with the measured $E_g = 3.23$ eV by Tauc's formula. Table 1 summarizes the optical bandgaps $E_g$ and particle sizes $d$ of Ag, ZnO, and Ag@ZnO NPs synthesized by the presented and other methods. The measured bandgaps are comparable to the reported ones, indicating our measured results are reliable.

## 3.5 Nonlinear optical properties

To extract the nonlinear optical coefficients and to gain an insight into the underlying mechanisms of the observed optical nonlinearities in nanomaterial dispersions, we carried

**Table 1** The optical bandgaps $E_g$ and particle sizes $R$ of Ag, ZnO, and Ag@ZnO NPs

| Samples | $E_g$ (eV) | $R$ (nm) | References |
|---|---|---|---|
| Ag NPs | 3.23 | 20 | This work |
| | 3.10 | 40–50 | [38] |
| ZnO NPs | 3.78 | 65 | This work |
| | 3.83 | 18 | [39] |
| Ag@ZnO NPs | 3.94 | 24 | This work |
| | 3.24 | 27–52 | [40] |

out the closed- and open-aperture Z-scan experiments at different levels of intensities. Besides, to exclude the optical nonlinearity arising from the solvent, we conducted Z-scan experiments on the pure deionized water in quartz cell. It is found that no Z-scan signal for the solvent was detected under our experimental condition. Evidently, the measured optical nonlinearities only originate from the nanomaterial itself.

Because all the measured open-aperture (or closed-aperture) Z-scan traces at different intensities are very similar in configuration, as an example, Fig. 6 illustrates only the open-aperture (by filled circles) and closed-aperture (by open circles) Z-scan traces measured at $I_0 = 78.2$ GW/cm$^2$ for aqueous solutions of Ag, ZnO, and Ag@ZnO NPs. Obviously, the absorptive nonlinearity of the three samples can be safely ignored because no peak or valley was detected in the open-aperture Z-scan traces. As shown in Fig. 6, all the closed-aperture Z-scan traces have the characteristics of symmetrical valley-to-peak configuration, indicating that three samples exhibit positive refractive nonlinearity. Furthermore, it is shown that the closed-aperture Z-scan signal increases in the order of NPs ZnO < Ag < Ag@ZnO. In a word, the as-synthesized three NPs possess purely third-order nonlinear refraction effect under the limitation of $I_0 \leq 78.2$ GW/cm$^2$.

From Fig. 6, one concludes that the absorptive nonlinearity of three NPs is negligible. This is anticipated for the following reasons: (1) the saturable absorption becomes negligible owing to insignificant linear absorption at 800 nm (see Fig. 5a); (2) two-photon absorption (2PA) is forbidden because the excitation photon energy ($h\nu = 1.56$ eV) and the bandgap $E_g$ (see Fig. 5b) of three NPs do not satisfy the 2PA requirement ($h\nu < E_g < 2h\nu$); and (3) three-photon absorption (3PA) is ignored under the excitation of relatively low intensity ($I_0 \leq 78.2$ GW/cm$^2$), although the 3PA requirement ($2h\nu < E_g < 3h\nu$) is satisfied.

For the sample exhibiting pure refractive nonlinearity induced by ultrafast laser pulses, the closed-aperture Z-scan normalized energy transmittance can be found as [41]

$$T(x,S) = \frac{1}{S}\left\{1 - \sum_{m,m'=0}^{\infty} \frac{\Delta\phi_0^{m+m'}(1-S)^{\lambda_{mm'}}\cos\psi_{mm'}}{m!m'!(m+m'+1)^{3/2}(x^2+1)^{m+m'}}\right\}, \quad (1)$$

where

$$\lambda_{mm'} = \frac{(m+m'+1)(x^2+1)[x^2+(2m+1)(2m'+1)]}{[x^2+(2m+1)^2][x^2+(2m'+1)^2]}, \quad (2)$$

$$\psi_{mm'} = (m-m')\left\{\frac{\pi}{2} - \frac{2(m+m'+1)x(x^2+1)\ln(1-S)}{[x^2+(2m+1)^2][x^2+(2m'+1)^2]}\right\}. \quad (3)$$

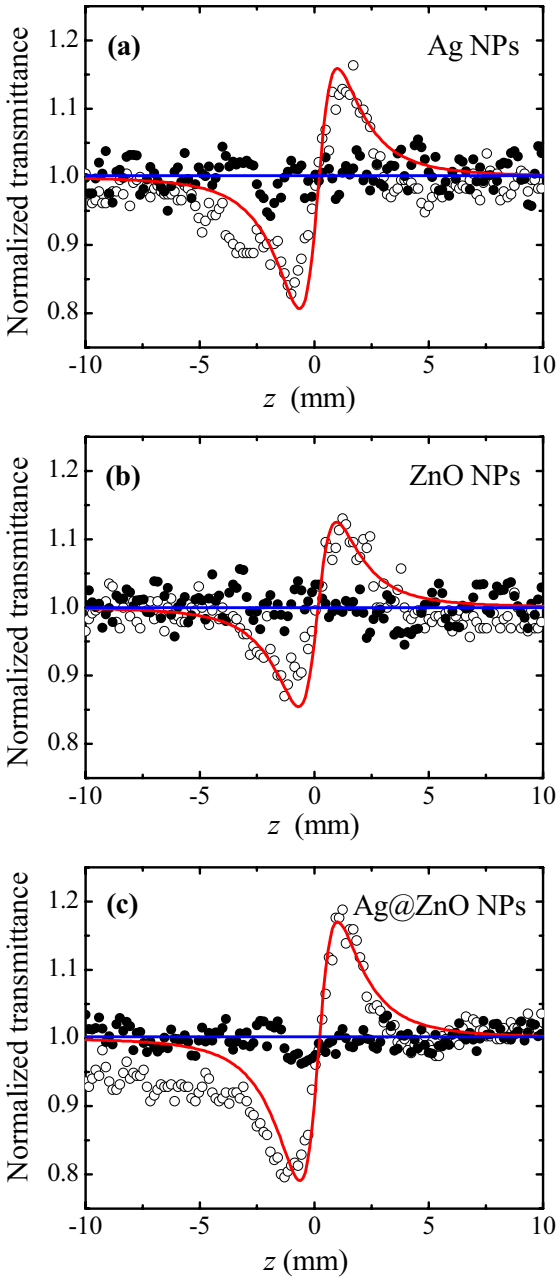


**Fig. 6** Examples of Z-scans measured at $I_0 = 78.2$ GW/cm$^2$ for aqueous suspensions of **a** Ag NPs, **b** ZnO NPs, and **c** Ag@ZnO NPs. Open and filled circles are the closed- and open-aperture Z-scans, respectively; while the solid lines are the best-fit curves simulated by Eq. (1)

Here, $\Delta\phi_0 = 2\pi n_2 I_0 L_{\text{eff}}/\lambda$, $L_{\text{eff}} = [1-\exp(-\alpha_0 L)]/\alpha_0$, $x = z/z_0$, and $z_0 = \pi\omega_0^2/\lambda$. $n_2$, $\alpha_0$, and $L$ are the third-order nonlinear refraction index, the linear absorption coefficient, and the physical thickness of the sample, respectively.

Using Eq. (1), we fit the measured closed-aperture Z-scan traces at different levels of $I_0$. As shown in Fig. 7, the extracted values of $n_2$ for three suspensions are all independent of the intensity $I_0$. Evidently, the observed refractive

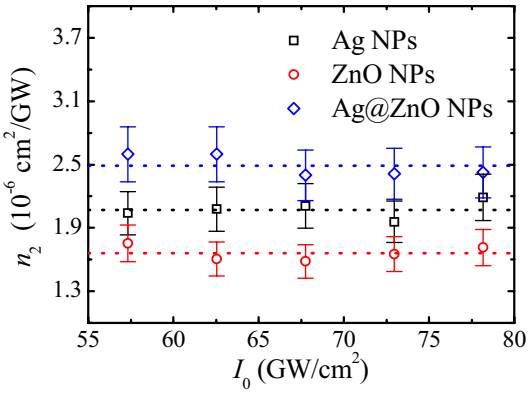


**Fig. 7** Intensity dependence of nonlinear refractive indexes for aqueous suspensions of Ag, ZnO, and Ag@ZnO NPs. The dotted lines are for guidance to the eyes

**Table 2** Femtosecond optical nonlinearities of Ag, ZnO, and Ag@ZnO NPs at the wavelength of 800 nm

| Samples | $n_2$ (cm$^2$/GW) | References |
|---|---|---|
| Ag NPs | $2.07\times10^{-6}$ | This work |
| | $1.9\times10^{-6}$ | [42] |
| ZnO NPs | $1.66\times10^{-6}$ | This work |
| | $1.6\times10^{-6}$ | [43] |
| Ag@ZnO NPs | $2.49\times10^{-6}$ | This work |

nonlinearity only originates from the third-order nonlinear refraction effect. The measured $n_2$ values for Ag, ZnO, and Ag@ZnO NPs are summarized in Table 2. For comparison, Table 2 also lists the nonlinear refractive indexes of Ag and ZnO NPs at 800 nm under the excitation of femtosecond laser pulses. Obviously, the measured values of $n_2$ for Ag and ZnO NPs are in good agreement with the ones reported previously [42, 43].

The underlying mechanisms of the observed refractive nonlinearities in three NPs are described in the following. As well known, ultrafast femtosecond pulses can eliminate the contribution to the refractive nonlinearity from molecular reorientation, electrostriction, and population redistribution because those effects have a characteristic response time much longer than 170 fs. Hence, in the femtosecond regime, the third-order refractive nonlinearity mainly originates from the distortion of the electron cloud. Besides, the cumulative thermal effect is negligible because the experiments were performed at a low repetition frequency of 1 kHz. Accordingly, the measured $n_2$ gives evidence of the electronic origin of refractive nonlinearity in Ag, ZnO, and Ag@ZnO NPs with the nonlinear response time of several hundred femtoseconds.

From Fig. 7, one easily finds that the nonlinear refraction index $n_2$ increases in the order of NPs ZnO < Ag < Ag@ZnO. The observed enhancement in the refractive nonlinearity of Ag@ZnO core–shell nanostructure can be explained by the following reasons: (1) the enhancement of nonlinear optical response is due to the intrinsic large nonlinearity of a composite material and coupling of dipole modes [23]; and (2) metal Ag NPs coated by dielectric ZnO materials exhibit enhanced nonlinear optical properties due to the local field enhancement of the metal Ag NPs [16].

Finally, we discuss the nonlinear optical property of Ag@ZnO core–shell NPs for potential applications in ultrafast all-optical switching. For realization of all-optical switching, nonlinear optical materials should satisfy the following requirements: (1) large nonlinear refraction index and ultrafast response time, and (2) low absorption losses due to both linear and nonlinear absorptions. From the linear absorption spectra (see Fig. 5a) and Z-scan measurements (see Fig. 6c), one concludes that the Ag@ZnO core–shell NPs have large electronic nonlinearity and low absorption losses due to both linear and nonlinear absorptions at 800 nm. The nonlinear response time of synthesized NPs exhibiting electronic nonlinearity is about several hundred femtoseconds, which is consistent with ~ 210 fs for Ag–BaO composite thin films [44] and ~ 250 fs for ZnO composite nanoparticles [45]. We estimate the all-optical switching time in core–shell NPs to be few picoseconds from the ones reported previously for silicon-based photonic crystal [46]. The results suggest that this material is a promising candidate for application in ultrafast all-optical switching.

## 4 Conclusion

In summary, we have respectively synthesized single NPs (i.e., Ag and ZnO NPs) and Ag@ZnO core–shell nanostructures by one-step and two-step PLAL methods. We have investigated the structural, morphological, componential, and optical properties of as-synthesized NPs by XRD, TEM, EDS, and UV–Vis absorption, respectively. It is confirmed that the high purity Ag@ZnO core–shell nanostructure was indeed synthesized by the two-step PLAL method. More importantly, we have exploited the third-order nonlinear optical properties of aqueous dispersions of Ag, ZnO and Ag@ZnO NPs by performing the femtosecond-pulsed Z-scan measurements in the near infrared region. It is shown that three NPs exhibit positive refractive nonlinearity in the absence of nonlinear absorption and the third-order nonlinear refraction index increases in the order of NPs ZnO < Ag < Ag@ZnO. We have discussed the underlying mechanisms of the observed optical nonlinearities of nanomaterial dispersions. Large refractive nonlinearity and low absorption losses due to both linear and nonlinear absorptions at 800 nm suggest that the Ag@ZnO core–shell

nanostructures would be desirable for potential applications in ultrafast all-optical switching.

**Acknowledgements** This work was supported by the National Science Foundation of China (Grant nos: 11174160, 11474052) and Natural Science Foundation of Jiangsu Province, China (BK20171364).

## References

1. R.G. Chaudhuri, S. Paria, Core/shell nanoparticles: classes, properties, synthesis, mechanisms, characterization, and applications. Chem. Rev. **112**, 2373–2433 (2011)
2. Y. Chen, H. Wu, Z. Li, P. Wang, L. Yang, Y. Fang, The study of surface plasmon in Au/Ag core/shell compound nanoparticles. Plasmonics **7**, 509–513 (2012)
3. P. Guo, D. Sikdar, X. Huang, K.J. Si, W. Xiong, S. Gong, L.W. Yap, M. Premaratned, W. Cheng, Plasmonic core–shell nanoparticles for SERS detection of the pesticide thiram: size-and shape-dependent Raman enhancement. Nanoscale **7**, 2862–2868 (2015)
4. M.B. Gawande, A. Goswami, T. Asefa, H. Guo, A.V. Biradar, D.L. Peng, R. Zboril, R.S. Varma, Core–shell nanoparticles: synthesis and applications in catalysis and electrocatalysis. Chem. Soc. Rev. **44**, 7540–7590 (2015)
5. H. Mei, W. Wu, B. Yu, H. Wu, S. Wang, Q. Xia, Nonenzymatic electrochemical sensor based on Fe@Pt core–shell nanoparticles for hydrogen peroxide, glucose and formaldehyde. Sens. Actuators B Chem. **223**, 68–75 (2016)
6. G. Cho, M. Jung, H. Yang, B. Lee, J.H. Song, Photonic crystals with tunable optical stop band through monodispersed silica–polypyrrole core–shell spheres. Mater. Lett. **61**, 1086–1090 (2007)
7. P. Rai, S.M. Majhi, Y.T. Yu, J.H. Lee, Synthesis of plasmonic $Ag@SnO_2$ core–shell nanoreactors for xylene detection. RSC Adv. **5**, 17653–17659 (2015)
8. M. Tsuji, S. Hikino, R. Tanabe, M. Matsunagaa, Y. Sanod, Syntheses of Ag/Cu alloy and Ag/Cu alloy core Cu shell nanoparticles using a polyol method. Cryst. Eng. Comm. **12**, 3900–3908 (2010)
9. M. Cazayous, C. Langlois, T. Oikawa, C. Ricolleau, A. Sacuto, Cu-Ag core–shell nanoparticles: a direct correlation between micro-Raman and electron microscopy. Phys. Rev. B **73**, 113402 (2006)
10. V. Amendola, M. Meneghettia, What controls the composition and the structure of nanomaterials generated by laser ablation in liquid solution? Phys. Chem. Chem. Phys. **15**, 3027–3046 (2013)
11. W.T. Nichols, T. Sasaki, N. Koshizaki, Laser ablation of a platinum target in water. I. Ablation mechanisms. J. Appl. Phys. **100**, 114911 (2006)
12. F. Mafuné, J.Y. Kohno, Y. Takeda, T. Kondow, Dissociation and aggregation of gold nanoparticles under laser irradiation. J. Phys. Chem. B **105**, 9050–9056 (2001)
13. J.S. Jeon, C.S. Yeh, Studies of silver nanoparticles by laser ablation method. J. Chin. Chem. Soc. **45**, 721–726 (1998)
14. I. Lee, S.W. Hana, K. Kim, Production of Au–Ag alloy nanoparticles by laser ablation of bulk alloys. Chem. Commun. **18**, 1782–1783 (2001)
15. S.C. Singh, R.K. Swarnkar, R. Gopal, Zn/ZnO core/shell nanoparticles synthesized by laser ablation in aqueous environment: optical and structural characterizations. Bull. Mater. Sci. **33**, 21–26 (2010)
16. A. Sakthisabarimoorthi, S.A. Martin Britto Dhas, M. Jose, Nonlinear optical properties of $Ag@SiO_2$ core–shell nanoparticles investigated by continuous wave He–Ne laser. Mater. Chem. Phys. **212**, 224–229 (2018)
17. R.T. Tom, A.S. Nair, N. Singh, M. Aslam, C.L. Nagendra, R. Philip, K. Vijayamohanan, T. Pradeep, Freely dispersible $Au@TiO_2$, $Au@ZrO_2$, $Ag@TiO_2$, and $Ag@ZrO_2$ core−shell nanoparticles: one-step synthesis, characterization, spectroscopy, and optical limiting properties. Langmuir **19**, 3439–3445 (2003)
18. Y. Zhao, S. Li, Y. Zeng, Y. Jiang, Synthesis and properties of Ag/ZnO core/shell nanostructures prepared by excimer laser ablation in liquid. APL Mater. **3**, 086103 (2015)
19. J. Li, S.K. Cushing, J. Bright, F. Meng, T.R. Senty, P. Zheng, A.D. Bristow, N. Wu, $Ag@Cu_2O$ core–shell nanoparticles as visible-light plasmonic photocatalysts. Acs Catal. **3**, 47–51 (2012)
20. A. Sakthisabarimoorthi, S.A. Martin Britto Dhas, M. Jose, Fabrication and nonlinear optical investigations of $SiO_2@Ag$ core–shell nanoparticles. Mater. Sci. Semicond. Process. **71**, 69–75 (2017)
21. K.W. Hu, T.M. Liu, K.Y. Chung, K.S. Huang, C.T. Hsieh, C.K. Sun, C.S. Yeh, Efficient near-IR hyperthermia and intense nonlinear optical imaging contrast on the gold nanorod-in-shell nanostructures. J. Am. Chem. Soc. **131**, 14186–14187 (2009)
22. L. Zhang, H. Dai, X. Wang, L. Yao, Z. Ma, J.B. Han, Nonlinear optical properties of Au–Ag core–shell nanorods for all-optical switching. J. Phys. D Appl. Phys. **50**, 355302 (2017)
23. P. Ma, D. Gao, Y. Ni, L. Gao, Enhancement of optical nonlinearity by core–shell bimetallic nanostructures. Plasmonics **11**, 183–187 (2016)
24. S. Perumbilavil, A. López-Ortega, G.K. Tiwari, J. Nogués, T. Endo, R. Philip, Enhanced ultrafast nonlinear optical response in ferrite core/shell nanostructures with excellent optical limiting performance. Small **14**, 1701001 (2018)
25. Y. Yang, M. Hori, T. Hayakawa, M. Nogami, Self-assembled 3-dimensional arrays of $Au@SiO_2$ core–shell nanoparticles for enhanced optical nonlinearities. Surf. Sci. **579**, 215–224 (2005)
26. Y.P.R. Grange, C.L. Hsieh, D. Psaltis, Nonlinear optical properties of core–shell nanocavities for enhanced second-harmonic generation. Phys. Rev. Lett. **104**, 207402 (2010)
27. E. Fazio, L. D'Urso, S. Santangelo, R. Saija, G. Compagnini, F. Neri, The activation of non-linear optical response in Ag@ZnO nanocolloids under an external highly intense electric field. Nuovo Cim. C **39**, 307 (2016)
28. M. Sheik-Bahae, A.A. Said, E.W. Van Stryland, High-sensitivity, single-beam $n_2$ measurements. Opt. Lett. **14**, 955–957 (1989)
29. M. Karimipour, M. Ebrahimi, Z. Abafat, M. Molaei, Synthesis of $Ag@TiO_2$ core–shells using a rapid microwave irradiation and study of their nonlinear optical properties. Opt. Mater. **57**, 257–263 (2016)
30. A.M. Mostafa, S.A. Yousef, W.H. Eisa, M.A. Ewaida, E.A. Al-Ashkar, Au@CdO core/shell nanoparticles synthesized by pulsed laser ablation in Au precursor solution. Appl. Phys. A **123**, 774 (2017)
31. A. Callegari, D. Tonti, M. Chergui, Photochemically grown silver nanoparticles with wavelength-controlled size and shape. Nano. Lett. **3**, 1565–1568 (2003)
32. J.R. Heath, Size-dependent surface-plasmon resonances of bare silver particles. Phys. Rev. B **40**, 9982 (1989)
33. H.R. Liu, G.X. Shao, J.F. Zhao, Z.X. Zhang, Y. Zhang, J. Liang, X.G. Liu, H.S. Jia, B.S. Xu, Worm-like Ag/ZnO core–shell heterostructural composites: fabrication, characterization, and photocatalysis. J. Phys. Chem. C **116**, 16182–16190 (2012)
34. J. Xiong, Q. Sun, J. Chen, Z. Li, S. Dou, Ambient controlled synthesis of advanced core–shell plasmonic Ag@ZnO photocatalysts. Cryst. Eng. Commun. **18**, 1713–1722 (2016)
35. X. Wang, X. Kong, Y. Yu, H. Zhang, Synthesis and characterization of water-soluble and bifunctional ZnO−Au nanocomposites. J. Phys. Chem. C **111**, 3836–3841 (2007)
36. J. Tauc, R. Grigorovici, A. Vancu, Optical properties and electronic structure of amorphous germanium. Phys. Stat. Sol. **15**, 627–637 (1966)

37. T.J. Jacobsson, T. Edvinsson, Absorption and fluorescence spectroscopy of growing ZnO quantum dots: size and band gap correlation and evidence of mobile trap states. Inorg. Chem. **50**(19), 9578–9586 (2011)
38. S.M. Hosseinpour-Mashkani, M. Ramezani, Silver and silver oxide nanoparticles: synthesis and characterization by thermal decomposition. Mater. Lett. **130**, 259–262 (2014)
39. L. Irimpan, V.P.N. Nampoori, P. Radhakrishnan, B. Krishnan, A. Deepthy, Size-dependent enhancement of nonlinear optical properties in nanocolloids of ZnO. J. Appl. Phys. **103**(3), 033105 (2008)
40. L. Muñoz-Fernandez, G. Alkan, O. Milošević, M.E. Rabanal, B. Friedrich, Synthesis and characterization of spherical core–shell Ag/ZnO nanocomposites using single and two–steps ultrasonic spray pyrolysis (USP). Catal. Today **321**, 26–33 (2019)
41. Y. Xue, Y. Wan, B. Gu, Femtosecond-pulsed Z-scan study on third-and fifth-order refractive nonlinearities in a side-chain azobenzene copolymer film. J. Nonlinear Opt. Phys. Mater. **27**, 1850007 (2018)
42. G.S. Boltaev, R.A. Ganeev, P.S. Krishnendu, S.K. Maurya, P.V. Redkin, K.S. Rao, K. Zhang, C.L. Guo, Strong third-order optical nonlinearities of Ag nanoparticles synthesized by laser ablation of bulk silver in water and air. Appl. Phys. A **124**(11), 766 (2018)
43. A. Rout, G.S. Boltaev, R.A. Ganeev, K.S. Rao, D. Fu, R.Y. Rakhimov, C.L. Guo, Low-and high-order nonlinear optical studies of ZnO nanocrystals, nanoparticles, and nanorods. Eur. Phys. J. D **73**(11), 235 (2019)
44. Q.F. Zhang, W.M. Liu, Z.Q. Xue, J.L. Wu, S.F. Wang, D.L. Wang, Q.H. Gong, Ultrafast optical Kerr effect of Ag–BaO composite thin films. Appl. Phys. Lett. **82**(6), 958–960 (2003)
45. R. Wang, X. Wu, B. Zou, L. Wang, S. Xie, J. Xu, W. Huang, Nonresonant optical nonlinearity of ZnO composite nanoparticles with different interfacial chemical environments. Mater. Res. Innov. **2**(1), 49–52 (1998)
46. A. Haché, M. Bourgeois, Ultrafast all-optical switching in a silicon-based photonic crystal. Appl. Phys. Lett. **77**(25), 4089–4091 (2000)